Advancing Bacterial Cellulose-Based Sensors: A Simplified 1D White-Box Model and Parametric Study for Single Carrier Mechanoelectric Transduction

Francesca Sapuppo[1], Luca Patanè[1], Riccardo Caponetto [1], Sara Sadat Housein[2], Salvatore Graziani[2], Antonino Pollicino[3] and Maria Gabriella Xibilia[1]

***Abstract*— Bacterial Cellulose (BC) functionalized with Ionic Liquids (ILs) is a promising candidate for sustainable electroactive sensors. While single-carrier transport models are well-established in piezoionic electroactive polymers, their applicability to BC-IL systems remains unverified. This study introduces a simplified 1D finite element model, significantly improving computational efficiency while preserving key physical insights. A detailed parametric analysis investigates the impact of different charge transport assumptions, revealing that single-carrier models are insufficient to fully describe the mechanoelectric transduction behavior. The results emphasize the necessity of a dual-carrier framework to accurately model BC-based transducers, offering a deeper understanding of multi-ionic interactions within the porous BC structure. By highlighting key mechanisms and limitations, this work provides a foundation for optimizing BC-IL sensors, preparing the way for more reliable and scalable bioelectronic applications.**

I. Introduction

The European Green Deal, introduced in December 2019, aims to position Europe as the first carbon-neutral continent, requiring one trillion euro in new green investments [1]. Meanwhile, global electronic waste has nearly doubled since 2010, reaching 62 million metric tons by 2022, with projections indicating an increase to 82 million metric tons by 2030. This growth raises significant environmental concerns due to the presence of non-recyclable and hazardous materials [2].

To address these challenges, polymers have been explored for sensor development and electronic applications. Ionic electroactive polymers (IEAPs) are particularly attractive due to their scalability, flexibility, and lightweight properties in motion-sensing systems. However, their environmental impact remains a concern. Bio-derived polymers provide a promising alternative by combining sustainability with the advantageous properties of synthetic polymers. Among these, cellulose has been widely investigated for its use in electronics and transducers.

[1]Francesca Sapuppo, Luca Patanè, e Maria Gabriella Xibilia are with Department of Electrical Engineering, University of Messina, Messina,Italy francesca.sapuppo@unime.it

[2]Sara Sadat Housein and Salvatore Graziani are with the Department of Electrical Electronics and Information Engineering, University of Catania, Catania, Italy

[3]Antonino Pollicino is with the Department of Civil Engineering and Architecture, University of Catania, Catania, Italy

This work was funded by Progetto Green SENSing systems based on Bacterial Cellulose (SENS-BC), Italian Ministry of University and Research, CUP J53D23003460006

Bacterial Cellulose (BC) has emerged as a sustainable alternative to plant-derived cellulose. Produced by bacteria such as *Acetobacter xylinum* and *Gluconacetobacter hansenii*, BC eliminates the need for deforestation, making it an environmentally friendly material. It features a porous, reticular structure with nanometric pores, enabling the incorporation and flow of ionic liquids (ILs) within its network. This unique interaction between the solid matrix and ILs is fundamental to charge transport and electromechanical behavior, making BC highly suitable for applications in electronics [3], actuators [4], and sensors [5]–[7].

When combined with ILs, BC becomes a strong candidate for organic electronics, sensors, and actuators. Understanding the underlying physical mechanisms governing its sensing and actuation behavior is crucial for optimizing design and improving rapid prototyping. Various modeling approaches are used to describe these phenomena, including black-box models [8], [9], gray-box models with integer or fractional orders [10], [11], and white-box models employing computational fluid dynamics (CFD) and finite element methods (FEM) in multiphysics domains [12]. Despite extensive research on the electromechanical transduction of ionic electroactive polymers, studies on their mechanoelectric transduction remain limited [13]–[16].

Focusing on white-box models, existing literature predominantly considers single ionic carrier models. This study investigates the feasibility of applying such models to BC-based sensors to determine whether they adequately describe the complex mechanoelectrical transduction processes. Additionally, while three-dimensional geometries are typically analyzed using FEM models, this work introduces a simplified approach based on multiple one-dimensional models. This strategy enables a faster computational analysis while assessing the validity of the introduced approximations, ultimately contributing to the development of more efficient models for BC-based sensors.

II. Material and Methods

A. BC-Based Sensor: Geometry and Manufacturing

The sensor structure based on BC comprises three distinct materials, each with unique physical and chemical properties. The fabrication process utilized CBP-GS010 BC films, supplied by BioFaber (Mesagne, Italy), with an approximate A4 size and thickness t_{BC} determined by the manufacturing procedure. The ionic liquid 1-Ethyl-3-Methylimidazolium

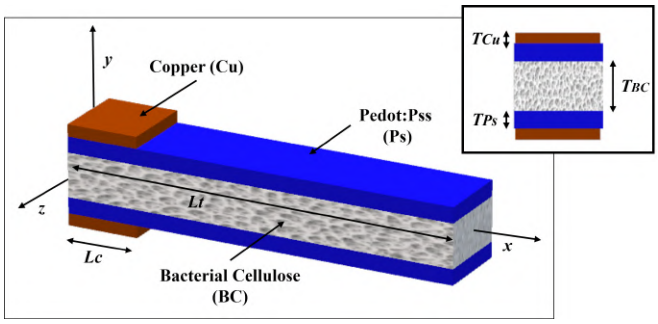

Fig. 1. Geometry of the BC-based sensor in the cantilever configuration

tetrafluoroborate ($EMIMBF_4$) was obtained from Alfa Aesar, while Poly(3,4-ethylene-dioxythiophene)-polystyrene-sulfonic acid (PEDOT-PSS) was sourced from H.C. Starck (1.3 wt% dispersion in water, Baytron P AG). In the sensor structure, BC serves as the bulk material, impregnated with $EMIMBF_4$ to enhance ionic conductivity. The impregnated BC is then coated on both sides with PEDOT-PSS films, which function as electrodes. The resulting BC-IL/PEDOT composite can be cut into strips of varying dimensions. The BC strip, functioning as a sensor, is configured in a cantilever setup, where it is fixed at one end and bends in response to applied force, generating an electrical signal at the electrodes. The device's geometry and parameters are illustrated in Fig. 1: W represents the sample width, L_c denotes the length of the clamped copper electrode, and L_t indicates the total sample length. The thicknesses of the BC, PEDOT, and copper electrodes are denoted as T_{BC}, T_{Ps}, and T_{Cu}, respectively. These parameters can be adjusted based on the fabrication process and intended application.

B. Experimental Setup and Acquisitions

The mechano-electric transduction properties of the BC-based sensor can be investigated by experiments for model validation. The experimental setup in Fig. 2 was designed to investigate the mechanical and electrical behavior of BC-based composite transducers configured in a cantilever arrangement. This configuration allowed the imposition of controlled mechanical vibrations on the transducer while simultaneously measuring its electrical response. The transducer was securely clamped at one end, referred to as the base clamp position, and its free end was equipped with two magnets, each with a diameter of 2 mm, positioned at a distance L_M from the base clamp. These magnets were used to facilitate the controlled application of external forces via an electromagnetic actuator. The actuator, driven by an Agilent 33220A signal generator, imposed tip displacement on the BC sensor by acting on the magnets. This setup allowed the application of sinusoidal forcing at a known frequency of the mechanical excitation. To monitor the mechanical response of the transducer, a laser displacement sensor (BAUMER OADM 12I6460 / S35A) was placed at a distance L_L from the base clamp position. The laser measured the deflection of the free end of the transducer, allowing for accurate assessment of the mechanical deformation. This experimental configuration provided a robust platform for evaluating the performance of BC-based transducers by correlating the imposed mechanical deformation with their corresponding electrical responses. The BC-based transducer's electrical response, specifically the open-circuit voltage, was measured directly using a digital oscilloscope (Agilent MSO7054A). The oscilloscope simultaneously captured the voltage signals from the transducer and the outputs from the laser displacement sensors, enabling a comprehensive analysis of the transducer electrical and mechanical behavior. Figure 3 presents an acquisition performed with an imposed sinusoidal deformation at a frequency of 40 Hz and an amplitude of $d_{\text{MAX}} = 0.45$ mm, measured at the laser point. The sensor voltage response exhibits a periodic signal with a peak amplitude of $V_{\text{max}} = 0.15$ mV, maintaining phase alignment with the input signal. This experimental dataset was utilized for model calibration and validation.

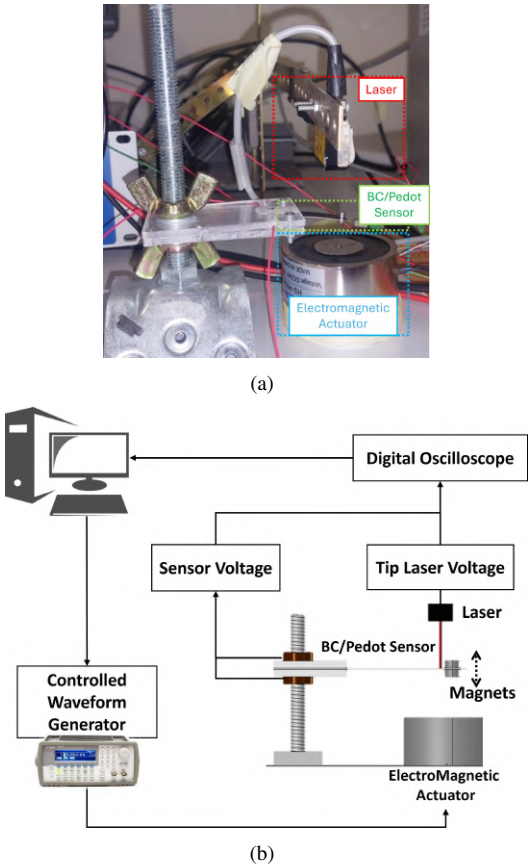

Fig. 2. Mechanical setup: (a) Laboratory setup. (c) Global schematic of the acquisition system

C. Multiphysics Based Model

The BC-based transducer operates as both a sensor and an actuator, converting mechanical deformation into electrical energy and vice versa. In sensing mode, when an external force ($\boldsymbol{F}$) is applied at the sensor tip, mobile cations ($EMIM^+$) and anions (BF_4^-) redistribute within the BC matrix. This ionic unbalance generates an electrical potential, which can be detected at the electrodes.

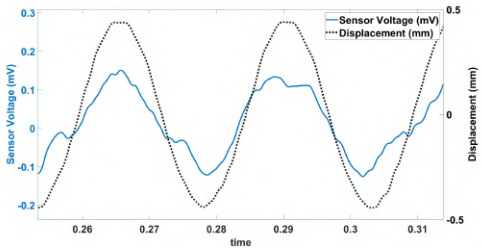

Fig. 3. Experimental acquisition of displacement and sensor voltage. The displacement input is a sinusoid with amplitude $d_{MAX} = 0.45mm$ at a frequency of $40Hz$

To model this behavior, a multiphysics approach is adopted, integrating three interdependent domains: mechanics, chemistry, and electricity. The physics is described by partial differential equations defined over the spatial domain, where $\boldsymbol{r}$ represents the coordinate vector (x, y, z) and t denotes time [14]. The mechanical model governs the structural deformation, the chemical model describes the ionic transport and current generation, while the electrical model determines the potential distribution within the sensor. The coupling between these domains forms the core of the modeling framework. The analysis assumes that materials are isotropic, homogeneous, temporally invariant, and linear to simplify the computations.

1) Mechanical Model: The structural behavior follows Newton's second law, relating the displacement (d) to the applied volumetric force (F):

$$\rho \frac{\partial^2 \boldsymbol{d}(\boldsymbol{r},t)}{\partial t^2} - \nabla \cdot c\nabla \boldsymbol{d}(\boldsymbol{r},t) = \boldsymbol{F}(\boldsymbol{r},t) \tag{1}$$

where ρ is the material density and c is the Navier constant. The volumetric strain ($dVol$) is linked to the displacement by:

$$dVol = \nabla \cdot \boldsymbol{d}(\boldsymbol{r},t). \tag{2}$$

The material pressure (p) is then expressed in terms of Young's modulus (E) and Poisson's ratio (ν):

$$p = \frac{E(1-\nu)}{(1+\nu)(1-2\nu)} dVol. \tag{3}$$

It is also related to the stress tensor components:

$$p = \frac{\sigma_{11} + \sigma_{22} + \sigma_{33}}{3} \tag{4}$$

Using the momentum conservation law, the relationship between the polymer pressure (p) and fluid pressure (P) is given by:

$$\nabla P = -\nabla p \tag{5}$$

2) Chemical Model: The transport of $EMIM^+$ cations and BF_4^- anions is governed by the Nernst-Planck equation:

TABLE I

GEOMETRICAL PARAMETERS.

Parameter description	Value	Unit
Total length, L	4	cm
Clamp region length, L_C	1.5	cm
Total width, W	1	cm
Thickness of BC, T_{BC}	320	um
Thickness of PEDOT, T_{PSS}	25	um
Distance between magnets and base, L_M	3.7	cm
Distance between laser reading point and base, L_L	3.2	cm

TABLE II

MECHANICAL PARAMETERS

Parameter description	Value	Unit
Young modulus of BC-PEDOT compound, E_{BC}	1.64	GPa
Poisson ratio of BC [17], ν_{BC}	0.01	-
Poisson ratio of PEDOT, ν_{PSS}	0.435	-
Mass density of BC, ρ_{BC}	0.904	g/cm^3
Mass density of PEDOT, ρ_{PSS}	1.28	g/cm^3

$$\frac{\partial C_i(\boldsymbol{r},t)}{\partial t} = \nabla \cdot \Big(D_i \nabla C_i(\boldsymbol{r},t) + z_i \mu_i F C_i(\boldsymbol{r},t) \nabla V(\boldsymbol{r},t) + \mu_i C_i(\boldsymbol{r},t) D_{v_i} \nabla P(\boldsymbol{r},t) \Big) \tag{6}$$

where i is the notation for the i^{th} specie; D_i is the diffusion coefficient; C_i the ion concentration; z_i the charge number; μ_i the mobility; F the Faraday constant; V the electric potential; and D_{v_i} the molar volume.

3) Electrical Model: The potential distribution V within the BC matrix is obtained using the Poisson equation:

$$-\epsilon_0 \epsilon_r \nabla^2 V(\boldsymbol{r},t) = \rho_0 + \sum_{i=1}^{N} z_i e C_i(\boldsymbol{r},t) \tag{7}$$

where ϵ_0 is the absolute dielectric constant, ϵ_r the relative dielectric constant, ρ_0 the permanent charge density and e is the elementary charge. The ion concentrations C_i establish the coupling with the chemical model in (6). The general form of the Nernst-Planck equation for the total flux $\boldsymbol{J_i}$ of the i^{th} ion species in (8) consists of three distinct components: diffusion, electromigration, and advection:

$$\boldsymbol{J_i} = -D_i \nabla C_i(\boldsymbol{r},t) - z_i \mu_i F C_i(\boldsymbol{r},t) \nabla V - \mu_i C_i(\boldsymbol{r},t) D_{v_i} \nabla P(\boldsymbol{r},t) \tag{8}$$

D. Parameters

Tables I through IV summarize the parameters used in the experimental and simulation setup. These include geometric dimensions, mechanical properties, electrochemical parameters, and electrical characteristics of the sensor. They are determined from experimental measurements or extracted from the literature. Any unknown parameters or additional scaling factors can be identified by aligning macroscopic model simulation results with experimentally observed field quantities.

TABLE III

CHEMICAL PARAMETERS.

Parameter description	Value	Unit
Initial ion concentration, C_0	740.88	mol/m^3
Cation diffusion constant, D_{cat}	4×10^{-10}	m^2/s
Anion diffusion constant, D_{an}	4.4×10^{-10}	m^2/s
Cation molar volume, $D_{v_{cat}}$	1.15×10^{-4}	m^3/mol
Anion molar volume, $D_{v_{an}}$	3.85×10^{-5}	m^3/mol
Cation charge number, Z_{cat}	1	-
Anion charge number, Z_{an}	-1	-
Temperature, T	298.15	K
Cation mobility, μ_{cat}	$D_{cat}/(R \cdot T)$	s·mol/kg
Anion mobility, μ_{an}	$D_{an}/(R \cdot T)$	s·mol/kg
Universal gas constant, R	8.31	J/(K·mol)
Cation mass, m_{cat}	111	g/mol
Anion mass, m_{an}	87	g/mol

TABLE IV

ELECTRICAL PARAMETERS.

Parameter description	Value	Unit
Effective absolute dielectric permittivity of BC-PEDOT compound, ϵ	5.8×10^{-2}	F/m

E. Simplified FEM Implementation

The white-box model is implemented through FEM simulations, which solve partial differential equations over both spatial and temporal domains. This method discretizes the spatial domain into finite elements, with each element approximating the solution locally. The mesh structure is formed by subdividing the domain into interconnected nodes, capturing the spatial variation of the solution and its properties. The model output provides a spatiotemporal distribution of key field variables, including displacement (d), cation and anion concentrations (C_i), and electric potential (V). A spatially simplified finite element model (1D FEM) was developed and solved in two sequential steps. First, the mechanical model was computed in a 2D domain to determine the pressure distribution within the material (p). The pressure values were extracted along three selected cutlines at 0.1 mm, 0.5 cm, and 1 cm from the fixed clamp and then converted into fluid pressure (P) using (5). These extracted pressure profiles were subsequently integrated into three separate 1D FEM models, which included the electrochemical physics domain to compute the potential field and determine the voltage at the electrode terminals. For simplicity, the three models were treated as uncoupled, neglecting the effect of PEDOT along the x-axis in the 1D model.

III. RESULTS AND DISCUSSION

This section presents the numerical analysis results, assessing the feasibility and limitations of the single-carrier model for BC-based sensors. The experimental setup described in Section II-B outlines the acquisition protocol and provides a validation dataset for the sensor's displacement input and voltage output (Fig. 3). The FEM implementation subsection details the 1D simplified numerical model developed to simulate the mechanoelectrical response of the system. The single carrier analysis explores different modeling configurations, the cases of mobile cation with a fixed anion and mobile anion with a fixed cation, comparing their influence on the generated electrical potential.

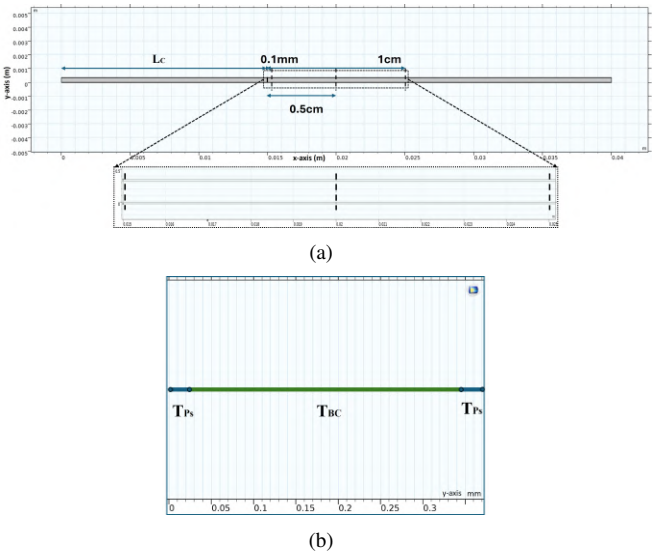

Fig. 4. Spatial Simplified FEM Model Geometry. (a) 2D geometry for the mecchanical domain model, (b) 1D geometry for the mechano-electrical trasduction model at the different y-axis cutlines

A. 2D Mechanical Model Solution

A simulation was conducted using COMSOL Multiphysics, applying a sinusoidal displacement signal at 40Hz with a maximum amplitude of $d_{\text{MAX}} = 0.45$ mm at the laser measurement point, according to the experimental dataset. The mechanical model described in Section II-C.1 was solved on a two-dimensional domain representing a cross-section of the real sensor, as illustrated in Fig. 4. The primary objective of this analysis was to compute the distribution of the field variable p, which serves as the coupling input for the mechanoelectrical model. From the 2D solution presented in Fig. 5(a), pressure values and their spatial gradients were extracted along specific cross-sections at 0.1 mm , 0.5 cm, and 1 cm from the fixed base L_C. As shown in Fig. 5(b) and (c), the pressure gradient in the x-axis direction is two orders of magnitude smaller than that in the y-axis direction. Consequently, the x-component contribution is negligible and is omitted from the Nernst-Planck equation in (6). This result supports the validity of the assumption that a reduction to a one-dimensional model along the y-axis provides a reasonable approximation.

B. 1D Single Carrier Analysis

The pressure profiles p extracted from the mechanical model over time were used as input for the chemical and electrical models, which were defined on a one-dimensional geometry. This approach enables a simplified yet insightful analysis of the coupling effects between mechanical deformation and ionic transport within the BC-based sensor.

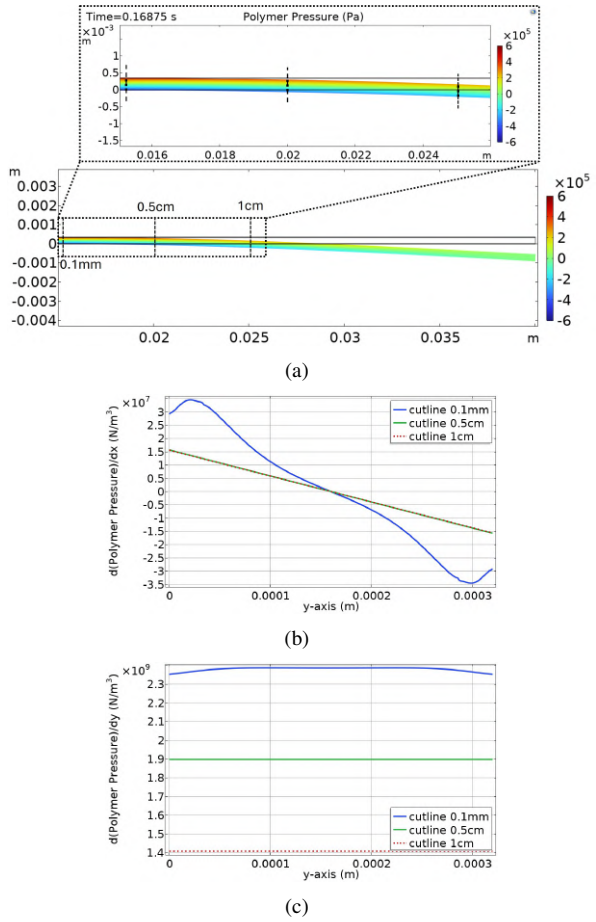

Fig. 5. Pressure field distribution in the polymer and its spatial variation: (a) 2D pressure map, (b) spatial gradient in the y direction for the selected y-axis cross-sections, and (c) spatial gradient in the x direction for the selected y-axis cross-sections.

In this paper, building on the state-of-the-art [13]–[15], we adopt a single mobile ionic charge carrier approximation while assuming the other remains fixed within the BC fibers. Two possible approaches are considered: either maintaining a constant concentration for the fixed carrier ($C_i = C_0$) as in 6(a) and(b) or allowing its concentration to vary with the volumetric strain ($C_i = C_0(1 - dVol)$) as in Fig. 7(a) and (b). These results clearly show that, in every scenario, the mechanoelectrical response is more pronounced near the fixed clamp, where the cantilever curvature is highest. Additionally, it is evident that both the amplitude and phase of the mechanoelectrical response vary across different scenarios. In the case where the immobile ions remain at a constant concentration (Fig. 6), the amplitude and delay obtained using nominal parameters do not match the experimentally observed values. Specifically, for the fixed anion scenario, the simulated response yields $V_{\text{MAX}} = 60\mu$V with a phase delay of 300°, whereas for the fixed cation case, the response reaches $V_{\text{MAX}} = 25\mu$V with an 80° delay. These values significantly deviate from the experimental dataset, which presents $V_{\text{MAX}} = 0.15$ mV with no phase delay (0°). On the other hand, when the fixed ion concentration depends on the volumetric strain (Fig. 7), the response is significantly overestimated. Specifically, for the fixed anion scenario, the simulated response reaches $V_{\text{MAX}} = 20$ mV with a phase delay of 180°, while for the fixed cation case, the response attains $V_{\text{MAX}} = 18$ mV, remaining in phase with the input signal. These deviations highlight the limitations of this assumption in accurately capturing the real mechanoelectrical transduction behavior of the BC-based sensor. The amplitude overestimation aligns with literature values, reporting voltage magnitudes in the order of tens of millivolts for sensors using EMIMBF_4 as the ionic liquid, where anions are immobilized within the bulk lattice [15]. These discrepancies underscore the distinct contributions of anion and cation mobility to the overall mechanoelectrical response. Furthermore, Fig. 8 shows how as the cation diffusion coefficient D_{cat} increases in the scenario where $C_{an} = C_0$, the simulated response can be tuned to match the experimentally obtained response. However, the phase discrepancy persists. Although these approximations do not fully capture the complexity of real ionic liquid behavior in BC, they serve as limiting cases to analyze the fundamental transport mechanisms. This investigation provides valuable insights into the multi-charge dynamics of ionic liquids within the porous BC structure, contributing to a more comprehensive understanding of mechanoelectrical transduction in these materials.

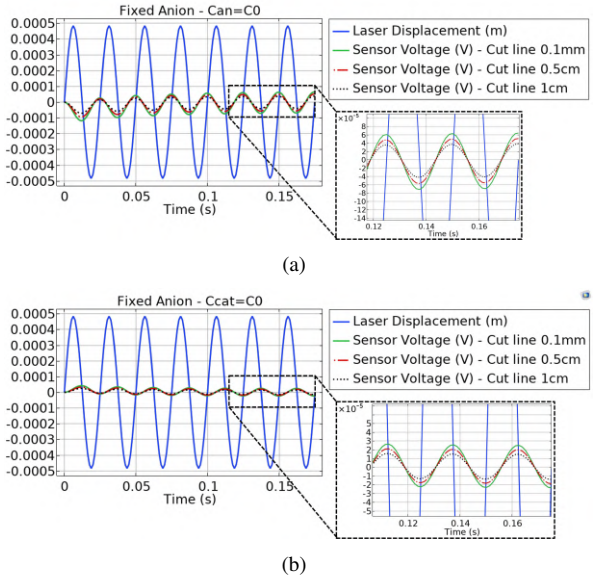

Fig. 6. BC-Sensor simulation under different conditions: (a) fixed anions with $C_{an} = C_0$, (b) fixed cations with $C_{cat} = C_0$.

IV. Conclusions

This study challenges the adequacy of single-carrier models for BC-based sensors, revealing their limitations in capturing the complex interplay of ion transport and mechano-electric transduction. While widely applied in electroactive polymer research, these models fail to reproduce experimental responses in BC-IL systems, where both cation and anion dynamics contribute to charge transport.

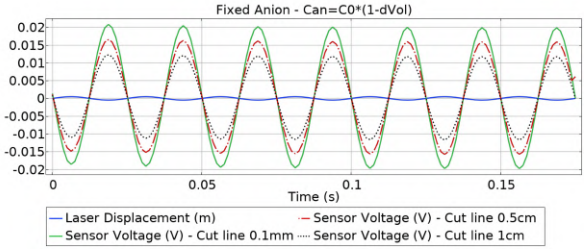

(a)

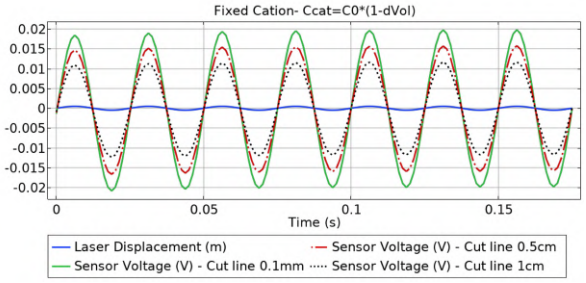

(b)

Fig. 7. BC-Sensor simulation under different conditions: (a) fixed anions with $C_{an} = C_0(1 - dVol)$, (b) fixed cations with $C_{cat} = C_0(1 - dVol)$.

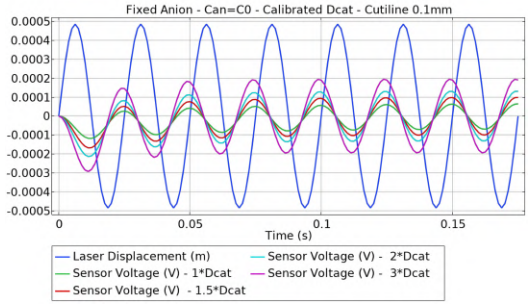

(a)

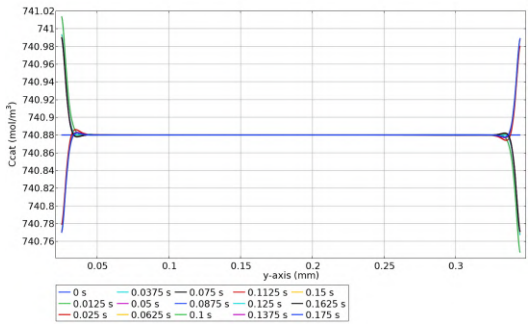

(b)

Fig. 8. Model calibration by varying the diffusion coefficient D_{cat} with multiplication factors (1, 1.5, 2, 3) along the 0.1 mm y-axis cutline. (a) Sensor voltage response, (b) Cation distribution at the peak of the sensor voltage response for $D_{cat} \times 3$.

To explore the fundamental transport mechanisms, an extensive parametric study was conducted, examining key factors influencing the mechanoelectric response. This analysis not only highlights the discrepancies in current modeling approaches but also provides valuable insights into the multi-charge dynamics within the porous BC structure. By identifying the critical parameters that govern sensor behavior, these findings establish a clear direction for future research, emphasizing the need for a dual-carrier model.

Embracing this refined perspective will lead to more accurate predictive tools, ultimately enabling BC-based transducers to reach their full potential in bioelectronics and sustainable sensing technologies.

REFERENCES

[1] A. D'Alfonso, "European green deal investment plan," European Parliament, Tech. Rep., 2020.

[2] B. Alves, "Global e-waste generation 2010-2022," Statista, Tech. Rep., 2024.

[3] J. D. Yuen, L. C. Shriver-Lake, S. A. Walper, D. Zabetakis, J. C. Breger, and D. A. Stenger, "Microbial nanocellulose printed circuit boards for medical sensing," *Sensors*, vol. 20, no. 7, 2020.

[4] S.-S. Kim, J.-H. Jeon, C.-D. Kee, and I.-K. Oh, "Electro-active hybrid actuators based on freeze-dried bacterial cellulose and pedot:pss," *Smart Materials and Structures*, vol. 22, no. 8, p. 085026, jul 2013.

[5] J. Huang, M. Zhao, Y. Hao, and Q. Wei, "Recent advances in functional bacterial cellulose for wearable physical sensing applications," *Advanced Materials Technologies*, vol. 7, no. 1, p. 2100617, 2022.

[6] Y.-H. Wang, P. Song, X. Li, C. Ru, G. Ferrari, P. Balasubramanian, M. Amabili, Y. Sun, and X. Liu, "A paper-based piezoelectric accelerometer," *Micromachines*, vol. 9, no. 1, 2018.

[7] G. Di Pasquale, S. Graziani, A. Pollicino, and C. Trigona, "Performance characterization of a biodegradable deformation sensor based on bacterial cellulose," *IEEE Transactions on Instrumentation and Measurement*, vol. 69, no. 5, pp. 2561–2569, 2020.

[8] L. Yang, Y. Yang, and H. Wang, "Modeling and control of ionic polymer metal composite actuators: A review," *European Polymer Journal*, vol. 186, p. 111821, 2023.

[9] M. Calapristi, L. Patanè, F. Sapuppo, and M. G. Xibilia, "Interpretability analysis of symbolic regression models for dynamical systems," in *2024 International Conference on Control, Automation and Diagnosis (ICCAD)*, 2024, pp. 1–6.

[10] R. Caponetto, S. Graziani, F. Sapuppo, and V. Tomasello, "An Enhanced Fractional Order Model of Ionic Polymer-Metal Composites Actuator," *Advances in Mathematical Physics*, vol. 2013, pp. 1–6, August 2013.

[11] R. Caponetto, S. Graziani, F. Pappalardo, and F. Sapuppo, "Identification of ipmc nonlinear model via single and multi-objective optimization algorithms," *ISA Transactions*, vol. 53, no. 2, pp. 481–488, 2014.

[12] R. Caponetto, V. De Luca, G. Di Pasquale, S. Graziani, F. Sapuppo, and E. Umana, "A multiphysics frequency-dependent model of an ip^{2}c actuator," *IEEE Transactions on Instrumentation and Measurement*, vol. 63, no. 5, pp. 1347–1355, 2014.

[13] D. Pugal, P. Solin, A. Aabloo, and K. J. Kim, "IPMC mechanoelectrical transduction: its scalability and optimization," *Smart Mater. Struct.*, vol. 22, no. 12, p. 125029, Dec. 2013.

[14] D. Pugal, *Physics based model of ionic polymer-metal composite electromechanical and mechanoelectrical transduction*. University of Nevada, Reno, 2012.

[15] Q. He, D. Vokoun, T. Stalbaum, K. J. Kim, A. I. Fedorchenko, X. Zhou, M. Yu, and Z. Dai, "Mechanoelectric transduction of ionic polymer-graphene composite sensor with ionic liquid as electrolyte," *Sensors and Actuators A: Physical*, vol. 286, pp. 68–77, 2019.

[16] L. Patanè, F. Sapuppo, G. Calapristi, Di Pasquale, Marco, S. Graziani, A. Pollicino, C. Trigona, and M. G. Xibilia, "A multiphysics framework for bacterial cellulose sensor modeling," in *2024 IEEE International Conference on Metrology for eXtended Reality, Artificial Intelligence and Neural Engineering*, 2024.

[17] P. Lopez-Sanchez, M. Rincon, D. Wang, S. Brulhart, J. R. Stokes, and M. J. Gidley, "Micromechanics and poroelasticity of hydrated cellulose networks," *Biomacromolecules*, vol. 15, no. 6, pp. 2274–2284, June 2014.